Mineralogical Magazine, October 1998, Vol. 62(5), pp. 617–638

Polymorphic transformations between olivine, wadsleyite and ringwoodite: mechanisms of intracrystalline nucleation and the role of elastic strain

LJUBA KERSCHHOFER[1†], CATHERINE DUPAS[1], MING LIU[2], THOMAS G. SHARP[1*], WILLIAM B. DURHAM[3] AND DAVID C. RUBIE[1]

[1] Bayerisches Geoinstitut, Universität Bayreuth, D-95440 Bayreuth, Germany
[2] Department of Earth, Atmospheric and Planetary Sciences, Massachusetts Institute of Technology, Cambridge, MA 02139, USA
[3] Lawrence Livermore National Laboratory, PO Box 808, Livermore, CA 94550, USA

ABSTRACT

Kinetic models and rate equations for polymorphic reconstructive phase transformations in polycrystalline aggregates are usually based on the assumptions that (a) the product phase nucleates on grain boundaries in the reactant phase and (b) growth rates of the product phase remain constant with time at fixed *P-T*. Recent observations of experimentally-induced transformations between $(Mg,Fe)_2SiO_4$ olivine (α) and its high pressure polymorphs, wadsleyite (β) and ringwoodite (γ), demonstrate that both these assumptions can be invalid, thus complicating the extrapolation of experimental kinetic data. Incoherent grain boundary nucleation appears to have dominated in most previous experimental studies of the $\alpha-\beta-\gamma$ transformations because of the use of starting materials with small (<10–20 μm) grain sizes. In contrast, when large (0.6 mm) olivine single crystals are reacted, intracrystalline nucleation of both β and γ becomes the dominant mechanism, particularly when the *P-T* conditions significantly overstep the equilibrium boundary. At pressures of 18–20 GPa intracrystalline nucleation involves (i) the formation of stacking faults in the olivine, (ii) coherent nucleation of γ-lamellae on these faults and (iii) nucleation of β on γ. In other experiments, intracrystalline nucleation is also observed during the $\beta-\gamma$ transformation. In this case coherent nucleation of γ appears to occur at the intersections of dislocations with (010) stacking faults in β, which suggests that the nucleation rate is stress dependent. Reaction rims of β/γ form at the margins of the olivine single crystals by grain boundary nucleation. Measurements of growth distance as a function of time indicate that the growth rate of these rims decreases towards zero as transformation progresses. The growth rate slows because of the decrease in the magnitude of the Gibbs free energy (stored elastic strain energy) that develops as a consequence of the large volume change of transformation. On a longer time scale, growth kinetics may be controlled by viscoelastic relaxation.

KEYWORDS: phase transformations, olivine, wadsleyite, ringwoodite, subduction zones.

Introduction

THE kinetics of reconstructive polymorphic phase transformations between minerals are of considerable interest in mineralogy, petrology and geophysics. Experimentally-determined kinetic data for the aragonite to calcite transformation, for example, can be used to constrain pressure-temperature-time (*P-T-t*) paths followed by high-pressure metamorphic terrains during uplift to the Earth's surface, thus constraining the tectonic processes involved (Carlson and Rosenfeld, 1981; Liu and Yund, 1993). Kinetic data for the reverse reaction, calcite to aragonite, have been used to evaluate *P-T* conditions under which calcite can

† Present address: Inst. f. Planetologie WWU Münster, D-48149 Münster, Germany

* Present address: Department of Geology, Arizona State University, Tempe, AZ 85287-1404, USA

survive as a metastable phase within the aragonite stability field during high-pressure metamorphism (Hacker *et al.*, 1992). At the higher pressures of the Earth's mantle transition zone (at depths of 410–660 km), the polymorphic transformations of $(Mg,Fe)_2SiO_4$ olivine to its high-pressure polymorphs, wadsleyite and ringwoodite, are likely to be kinetically inhibited within slabs of subducting lithosphere because of low temperatures (Sung and Burns, 1976; Rubie and Ross, 1994; Daessler *et al.*, 1996). In order to evaluate the geophysical consequences of this behaviour, a quantitative understanding of the transformation kinetics is required, as discussed below. In addition, large rheological changes (weakening) may accompany polymorphic phase transformations as a result of a change in the deformation mechanism caused by grain size reduction (Vaughan and Coe, 1981; Rubie, 1983, 1984, 1990; Ito and Sato, 1991; Riedel and Karato, 1996). In order to understand the effects that phase transformations have on rheology, a quantitative understanding of the kinetics of nucleation and growth is required (e.g. Riedel and Karato, 1996).

The application of experimental kinetic data to geological processes normally requires large extrapolations in temperature and time. For such extrapolations to be reliable, rate equations which are based on the specific reaction mechanism must be used (Rubie and Thompson, 1985). The possibility that reaction mechanisms might be different in laboratory experiments and in nature (because of different *P-T* conditions and time-scales, for example) must also be considered. In these respects, polymorphic phase transformations are particularly attractive because their mechanisms are simple compared with those of metamorphic reactions involving multiple mineral (and fluid) phases. The rates of polymorphic reactions should therefore be relatively easy to quantify and to extrapolate to different *P-T* conditions using appropriate kinetic rate equations.

The polymorphic phase transformations which have been most widely studied experimentally with respect to understanding mechanisms and kinetics are aragonite to calcite (Carlson and Rosenfeld, 1981; Liu and Yund, 1993), calcite to aragonite (Hacker *et al.*, 1992), and olivine to wadsleyite and/or ringwoodite (for references, see below). On the basis of these studies, it has been concluded that the dominant transformation mechanism in polycrystalline aggregates involves (i) incoherent nucleation on grain boundaries and (ii) interface-controlled growth involving short-range ionic diffusion in the vicinity of the interphase boundary. (In contrast, diffusion-controlled growth involves long-range diffusion and is likely to occur when growth of the product phase involves a change in composition, such as a change in Fe/Mg ratio — see Christian, 1975; Rubie, 1993.) A rate equation which describes the extent of transformation as a function of time, formulated for the grain-boundary nucleation and interface-controlled growth mechanism (Cahn, 1956), is:

$$\xi(t) = 1 - \exp\left\{-\frac{6.7}{d}\int_0^{y'}[1-\exp(-Y_e)]dy\right\} \quad (1)$$

where

$$Y_e(t,y) = \pi\int_0^{t-t'}\dot{N}\left[\dot{x}^2(t-\tau)^2 - y^2\right]d\tau$$

In Equation (1), $\xi(t)$ is the volume fraction of the new phase (e.g. the fraction of aragonite in a partially-reacted calcite-aragonite mixture) at time t, d is the grain size of the reactant phase, $\dot{N}$ is the rate of nucleation on grain boundaries and $\dot{x}$ is the growth rate of the product phase. Of the other variables, τ is the time at which a nucleus forms, the dummy variable y is the distance of an imaginary plane from the grain boundary on which the new phase nucleated, y' is the growth distance after time t, and t' is the time a new grain takes to grow to radius y. Through the exponential terms, Equation (1) takes into account the impingement of growing grains which effectively reduces the dimensionality of growth as transformation proceeds. Equation (1), which is evaluated numerically, can be used to extrapolate kinetic data provided the dependencies of the nucleation and growth rates on pressure and temperature are known (e.g. Rubie *et al.*, 1990). This rate equation has also been modified to describe transformation rates under conditions of changing temperature and pressure (Rubie and Ross, 1994, with corrections given by Kirby *et al.*, 1996).

Equation (1) can be simplified to give the well-known 'Avrami' equation:

$$\xi(t) = 1 - \exp(-kt^n) \quad (2)$$

provided that either the nucleation rate is so fast that all nuclei form instantly ($n = 1$) or the

nucleation rate is so slow that it is approximately constant during transformation (n = 4) (Cahn, 1956). Although the parameters k and n are assumed to be constants at fixed conditions of pressure and temperature, this is only the case so long as one of the above assumptions remains valid. The use of Equation (2) for extrapolating kinetic data to different P-T conditions can therefore be unreliable (Rubie *et al.*, 1990).

Recent studies of the kinetics of polymorphic phase transformations have used Equation (1), or a similar rate equation, based on the assumption that nucleation only occurs on grain boundaries (Rubie *et al.*, 1990; Liu and Yund, 1993; Rubie and Ross, 1994; Kirby *et al.*, 1996). An additional assumption of these studies is that growth is interface-controlled and occurs at a constant rate at fixed P-T conditions. This assumption is based on measurements of the dimensions of small isolated grains of the product phase as a function of time (Carlson and Rosenfeld, 1981) and also on theoretical considerations which have led to the following rate equation (Turnbull, 1956; Christian, 1975):

$$\dot{x} = k_0 T \exp[-(\Delta H_a + PV^*)/RT][1 - \exp(\Delta G_r/RT)] \quad (3)$$

where $\dot{x}$ is the growth rate, k_0 is a constant, ΔH_a is the activation enthalpy for growth, V^* is the activation volume for growth, ΔG_r is the free energy change of reaction, and R is the gas constant. The first exponential in this equation is an Arrhenius term that describes the rate of thermally-activated diffusion of atoms at the interphase boundary. The second part of the equation, in square brackets, is a thermodynamic term which incorporates the effect of the driving force (change in Gibbs free energy) on the growth rate. At equilibrium conditions, the driving force is zero (ΔG_r = 0) so that the growth rate is also zero.

In addition to pressure and temperature, non-hydrostatic stress can have a large effect on transformation rates. For example, when subjected to very high shear stresses, olivine transforms rapidly to ringwoodite at temperatures at least 200°C lower than those required when the stress is near-hydrostatic in laboratory experiments (Wu *et al.*, 1993). However, the mechanisms responsible for this enhancement of transformation rates by stress are not clear.

In this contribution we present new experimental results on the mechanisms and kinetics of transformations between olivine, wadsleyite and ringwoodite at 15–20 GPa. We show that intracrystalline nucleation is an important process, in addition to grain boundary nucleation, and under certain conditions is likely to dominate the transformation kinetics. Secondly, we show that rates of interface-controlled growth do not remain constant but decrease sharply with time due to the accumulation of elastic strain. In addition, we provide some insight into how non-hydrostatic stress enhances transformation rates. These observations must be taken into account when extrapolating experimental data to predict transformation rates in the Earth and we conclude that current kinetic models, based on Equations (1) and (3), need to be revised.

$(Mg,Fe)_2SiO_4$ phase transformations

The most abundant mineral in the upper mantle, $(Mg,Fe)_2SiO_4$ olivine (α-phase), transforms to the high-pressure polymorphs wadsleyite (β-phase) and ringwoodite (γ-phase) with increasing depth in the transition zone (Akaogi *et al.*, 1989). The $\alpha \rightarrow \beta$ and $\beta \rightarrow \gamma$ phase transformations result in positive density changes of 6% and 2%, respectively. Along a normal mantle geotherm where temperatures are expected to be ~1500°C in the transition zone (Ito and Katsura, 1989), olivine is expected to transform to wadsleyite fairly close to equilibrium conditions at a depth of ~410 km (see Solomatov and Stevenson, 1994, for a discussion of the kinetics). In contrast, it has been suggested that the transformations will be kinetically inhibited in subduction zones where temperatures might be as low as 500–600°C at a depth of 400 km (Sung and Burns, 1976; Rubie and Ross, 1994; Kirby *et al.*, 1996; Daessler *et al.*, 1996). Consequently olivine might survive as a metastable phase to depths of 600 km or more before transforming directly to ringwoodite under conditions far from equilibrium (Fig. 1). The metastable persistence of olivine in subducting slabs has a number of geophysical consequences related to the buoyancy forces driving subduction (Ito and Sato, 1991), the state of stress in the slab (Goto *et al.*, 1987), the rheology of subducting lithosphere (Rubie, 1984; Karato, 1996; Riedel and Karato, 1996) and the origin of deep focus earthquakes (Green and Houston, 1995; Kirby *et al.*, 1996).

Because of the geophysical and geodynamical consequences of metastable olivine surviving to great depths in subducting slabs, there have been many experimental investigations of the mechan-

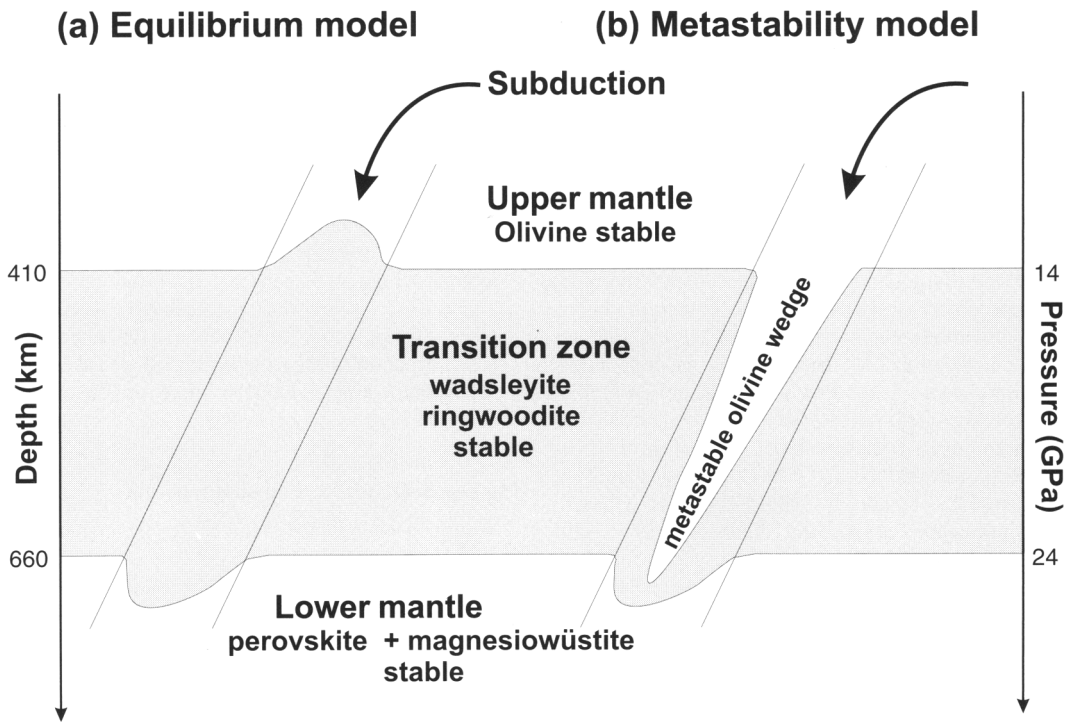

FIG. 1. Two models of a subducting slab: (*a*) In the equilibrium model the stability boundary of olivine is elevated to shallower depths than in the surrounding mantle because of the positive Clapeyron slope of the olivine to wadsleyite reaction. The stability boundary of ringwoodite is depressed into the lower mantle because the equilibrium phase boundary between ringwoodite and perovskite + magnesiowüstite has a negative Clapeyron slope. (*b*) In the metastability model the transition of olivine is kinetically inhibited and metastable olivine extends to a depth of 600 km or more in a wedge-shaped region. The location of the boundary of this wedge depends on the transformation kinetics and coincides approximately with a critical isotherm (Kirby *et al.*, 1996).

isms and, to a lesser extent, the kinetics of these phase transformations during the past 20 years. Until a few years ago, most studies were performed on analogue compositions, such as Mg_2GeO_4, Ni_2SiO_4 and Co_2SiO_4, because much lower pressures are required for transformation in these systems than for $(Mg,Fe)_2SiO_4$ (for references see Rubie, 1993). (Note that of these compositions, the β-phase structure is only stable in Co_2SiO_4.) Studies on $(Mg,Fe)_2SiO_4$ samples have been performed either in a multi-anvil press (Rubie and Brearley, 1990; Guyot *et al.*, 1991; Brearley *et al.*, 1992; Fujino and Irifune, 1992; Rubie and Brearley, 1994; Sharp and Rubie, 1995; Kerschhofer *et al.*, 1996; Martinez *et al.*, 1997) or in a diamond anvil cell (Lacam *et al.*, 1980; Boland and Liu, 1983; Furnish and Bassett, 1983; Madon *et al.*, 1989; Wu *et al.*, 1993). Transmission electron microscopy (TEM) has shown that the $\alpha-\beta-\gamma$ transformations can occur by two distinctly different mechanisms involving grain boundary nucleation and coherent intracrystalline nucleation respectively.

The grain boundary nucleation mechanism involves incoherent nucleation on grain boundaries and grain boundary triple junctions in the reactant phase (e.g. Brearley *et al.*, 1992). In the cases where the reactant and product phases have the same composition, it can be assumed that the growth of the product phases is interface-controlled. On the other hand, when reaction occurs in a two-phase field (e.g. $\alpha+\beta$ or $\beta+\gamma$ in the system $Mg_2SiO_4-Fe_2SiO_4$), growth should involve a change in Mg/Fe ratio (Akaogi *et al.*, 1989) and is therefore likely to be diffusion-controlled (Rubie, 1993). In experimental studies performed on univariant reactions (e.g. in

Mg_2SiO_4) it has been assumed that growth is interface-controlled (e.g. Rubie and Ross, 1994). Studies on $(Mg,Fe)_2SiO_4$ have sometimes reported different Mg/Fe values for reactant and product phases (e.g. Sharp and Rubie, 1995) and in these cases growth may be diffusion-controlled. There have been no determinations of the time-dependence of the growth rate, however, which might confirm these assumptions.

Because of similarities between the structures of the α-, β- and γ-phases (Fig. 2), it has been proposed by Hornstra (1960) and Poirier (1981) that transformations between these phases could occur by a shear or 'martensitic' mechanism involving co-operative atomic movements accomplished through the movement of partial dislocations. Transformations between β-phase and γ-phase only require cation redistribution because both phases have cubic close-packed oxygen sublattices (Fig. 2). The motion of 1/2 [101](010) partial dislocations in β-phase produces stacking faults with the γ-phase structure and the motion of $1/4<1\bar{1}2>\{110\}$ partial dislocations in γ-phase results in stacking faults with the β-phase structure (Madon and Poirier, 1983). The transformation of olivine to γ-phase by a shear mechanism is more complex and requires two steps because the structures are less similar (Fig. 2). To form a layer of γ-phase structure in the olivine lattice, the shear operation 1/12[013](100), creating $(100)_\alpha$ stacking faults, must be accompanied by the redistribution of the cations. In Poirier's model this is accomplished by the co-ordinated movement of the cations, i.e. by 'synchroshear' (Poirier, 1981).

Reported evidence for 'martensitic' $\alpha \rightarrow \gamma$ transformation in experimental studies has been indirect. From *in situ* x-ray diffraction experiments on fayalite, Furnish and Bassett (1983) inferred a two-stage shear mechanism from the sequential development of x-ray diffraction peaks with the second stage involving the cation rearrangement. Reported microstructural evidence consists primarily of observations of thin γ-phase lamellae in olivine which show the orientation relationship $(100)_\alpha // \{111\}_\gamma$ and $[001]_\alpha // <110>_\gamma$ (Lacam *et al.*, 1980; Boland and Liu, 1983; Madon *et al.*, 1989; Burnley, 1995; Martinez *et al.*, 1997). However, in none of these studies have $(100)_\alpha$ stacking faults or dissociated $[001]_\alpha$ dislocations been identified.

Evidence for the $\gamma \rightarrow \beta$ transformation by a shear mechanism was reported by Rubie and Brearley (1994) on the basis of high densities of stacking faults in γ-Mg_2SiO_4 which had been reacted in the β-phase stability field. However, experiments on β-phase reacted in the γ-phase stability field at comparable temperatures only produced evidence for incoherent grain boundary nucleation. These contrasting mechanisms may be the consequence of the number of independent slip systems available in the respective crystal structures, as discussed by Rubie and Brearley (1994).

It is important to identify the parameters that determine which transformation mechanism operates, because the kinetics clearly depend on the mechanism. Burnley (1990) showed that differential stress is an important controlling factor during the $\alpha-\gamma$ transformation in Mg_2GeO_4. Under high differential stresses ($\sigma_1 - \sigma_3 \geqslant 900$ MPa) and moderate temperatures (e.g. 600–900°C) coherent lamellae of γ-phase formed in α-Mg_2GeO_4 and were interpreted to indicate operation of the shear mechanism; in contrast, at high temperatures and low differential stresses olivine transformed to γ-phase by the grain boundary nucleation mechanism. In a more recent study (also on Mg_2GeO_4), Burnley (1995) showed that when the conditions overstep the α-γ equilibrium phase boundary by a large pressure interval (8–14 GPa), significant amounts of coherent intracrystalline transformation occur, presumably by the shear mechanism.

In this paper we present new results on the mechanisms of the $\alpha-\beta$, $\alpha-\gamma$ and $\beta-\gamma$ transformations in natural San Carlos olivine (Fo_{90}). We show that coherent intracrystalline nucleation is an important mechanism during the $\alpha \rightarrow \gamma$ transformation at pressure oversteps of $\geqslant$ 6 GPa and discuss microstructural observations which suggest that the mechanism is different to that proposed by Poirier (1981). We also identify a new mechanism of intracrystalline nucleation during the $\beta \rightarrow \gamma$ transformation which indicates that the kinetics are likely to be enhanced by differential stress. Finally we show that the growth rates of grain boundary nucleated grains can decrease drastically with reaction time, even though interface mechanisms are involved, because of the development of elastic strain.

Experimental

High-pressure experiments were performed using a 1200 tonne multianvil apparatus at the Bayerisches Geoinstitut. The pressure medium was an MgO octahedron with a 10 mm edge

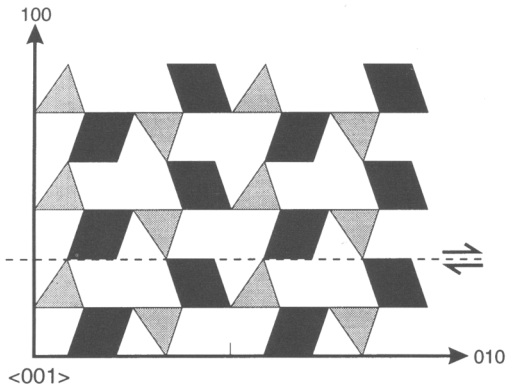

Olivine
Pbnm
O-lattice h.c.p.
in <100> direction

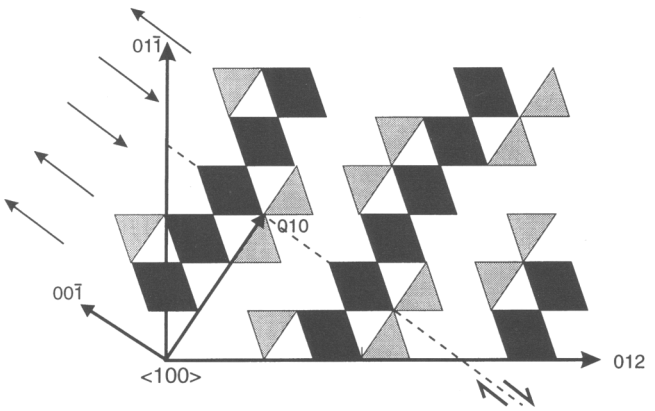

Wadsleyite
Imma
O-lattice c.c.p.
in <01$\bar{1}$> direction

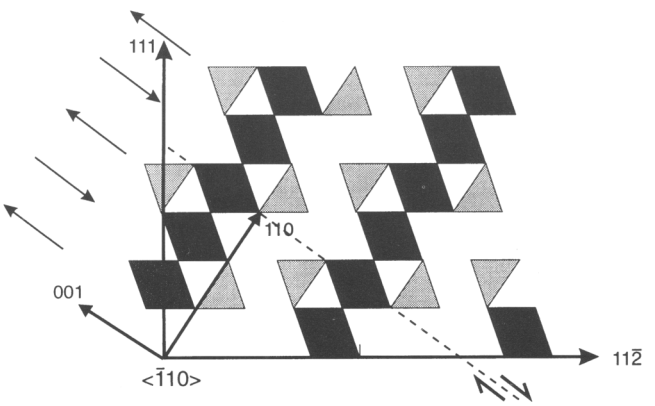

Ringwoodite
Fd3m
O-lattice c.c.p.
in <111> direction

length, which contained the sample, a cylindrical $LaCrO_3$ heater and a thermocouple (Fig. 3). Pressure was calibrated as a function of hydraulic oil pressure at 1200° and 1600°C using the coesite-stishovite and the Mg_2SiO_4 $\alpha-\beta$ and $\beta-\gamma$ phase transformations, with an uncertainty of ± 0.5 GPa (Canil, 1994). Because calibration did not involve a hot-pressing stage (see below), the pressure uncertainty in our kinetic experiments may be higher than ± 0.5 GPa (see discussion below). Temperature was measured with a W3%Re–W25%Re thermocouple without any correction for the possible effect of pressure.

We have performed a series of quasi-hydrostatic transformation experiments nominally in the γ-phase stability field and two non-hydrostatic experiments in the β and $\beta+\gamma$ stability fields; the purpose of the latter experiments was to investigate the effect of stress on transformation mechanisms. The samples for the quasi-hydrostatic experiments were contained in molybdenum capsules (1.6 mm diameter and 1.6 mm long). The capsules were placed in the centre of the pressure medium immediately adjacent to the thermocouple (Fig. 3*a*). In the sample assembly used for the non-hydrostatic experiments, the sample, together with a short dense aluminum piston, occupied the entire length of the octahedron and the thermocouple was placed directly in the powdered olivine sample (Fig. 3*b*).

The starting material for the quasi-hydrostatic experiments consisted of an oriented single crystal of San Carlos olivine (500 × 600 × 700 μm), with the composition $Mg_{1.8}Fe_{0.2}SiO_4$, that was contained in fine-grained matrix of San Carlos olivine powder plus 4 wt.% enstatite. After hot-pressing the matrix had a bimodal grain size distribution with a small proportion of 40 μm grains and a large proportion of 10 μm grains. The use of large single crystals enables the transformation processes to be studied over longer time periods than are possible for fine-grained samples

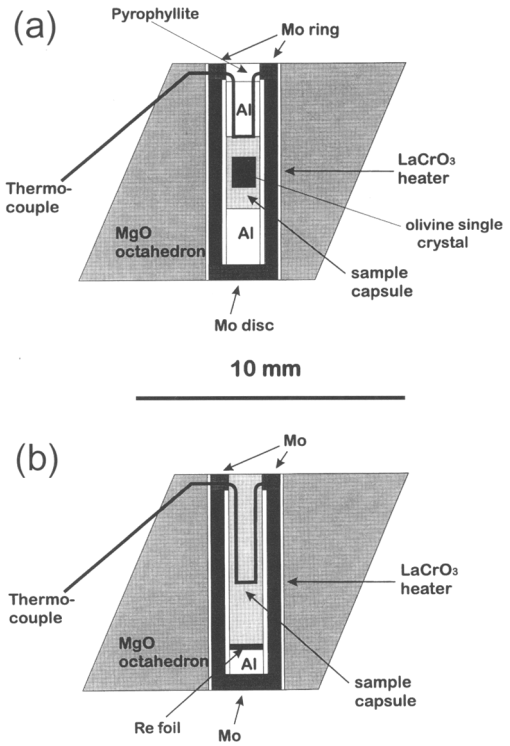

FIG. 3. Cross section of MgO octahedra used in the multianvil experiments: (*a*) In the quasi-hydrostatic assembly a molybdenum capsule containing the sample is 1.6 mm in diameter and 1.6 mm long and is located at the centre of the octahedron adjacent to the thermocouple. (*b*) In the non-hydrostatic assembly the sample (6.2 mm long × 1.6 mm diameter and contained in molybdenum foil) occupies most of the length of the octahedron together with a dense *aluminum piston* which imposes a differential stress on the sample. Rhenium foil of 10 μm thickness was placed between the sample and the piston to avoid chemical reaction.

FIG. 2. This simplified polyhedral representation modified from Madon and Poirier (1983) shows a comparison of the α-, β- and γ-phase structures as viewed along the $[001]_\alpha$, $[100]_\beta$ and $<\bar{1}10>_\gamma$ axes, respectively, with the dark grey rhombi representing the $(Mg,Fe)O_6$ octahedra and the light grey triangles representing the SiO_4 tetrahedra. The directions $[100]_\alpha$, $[01\bar{1}]_\beta$ and $<111>_\gamma$ are the stacking directions of the oxygen close-packed planes. The representation illustrates the similarity between the β- and γ-phase structures, which both belong to the family of spinelloids (Horiuchi *et al.*, 1980). The arrows on the left sides of the β- and γ-phase structures indicate how the basic structural component sheets of the cations are stacked along the $[010]_\beta$ and $<110>_\gamma$ directions, respectively. The code $\uparrow\uparrow$ represents a stacking obtained by a mirror operation, whereas $\uparrow\downarrow$ represents a stacking produced by a glide mirror operation (for details see Horiuchi *et al.*, 1982). The $(100)_\alpha$, $(010)_\beta$ and $\{110\}_\gamma$ planes (indicated by dashed lines) are the planes along which shear must occur during 'martensitic' transformations.

which react rapidly. The starting material for the non-hydrostatic experiments consisted of San Carlos olivine powder, which after hot-pressing had the same bimodal grain size distribution as that for the quasi-hydrostatic experiments but also contained a few larger (~60 μm) grains.

Kinetic studies should be performed on polycrystalline samples with well-equilibrated microstructures and low defect densities. The high defect densities and ultra-fine grain sizes produced by pressurising powdered samples (Brearley *et al.*, 1992) are likely to strongly enhance transformation rates. Therefore, we commenced each experiment by first pressurising the sample to 11 GPa at room temperature and then hot-pressing it in the olivine stability field, in most cases at 1200°C for 3 h (Fig. 4), to reduce defect densities and increase grain sizes through grain growth.

For the quasi-hydrostatic experiments, the sample was cooled to 600°C after hot pressing before being pressurised further to 18–20 GPa over a period of 120–160 min (Fig. 4). There was no transformation during pressurisation at this low temperature. Heating to high temperature to initiate transformation was rapid in all experiments (~2 min), thus enabling the time and pressure–temperature conditions at which transformation began to be well defined. Partial transformation to high-pressure polymorphs was studied through a series of experiments performed at 18 to 20 GPa and 600 to 1100°C for times ranging from 20 min to 23 h (Fig. 4, Table 1). In the non-hydrostatic experiments, after hot pressing (at 1250°C, 2h), the samples were pressurised to 15 or 16 GPa at 900°C and then held at these conditions for 30 minutes and 11 hours respectively (Fig. 4, Table 1). After rapid quenching and slow decompression, samples were prepared for examination by optical microscopy and transmission electron microscopy (TEM) (Philips CM20, 200 kV). Optical microscopy was used to obtain an estimate of the extent and homogeneity of transformation and to characterise large-scale microstructures. TEM was used to investigate the sizes and morphologies of the product grains, crystallographic orientation relationships and defect microstructures.

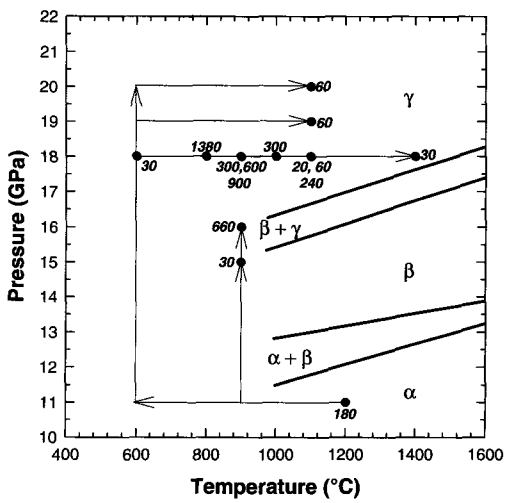

FIG. 4. Phase diagram for $Mg_{1.8}Fe_{0.2}SiO_4$ showing the stability fields of olivine (α), wadsleyite (β), and ringwoodite (γ) (after Katsura and Ito, 1989). The arrows indicate the *P–T–t* paths for our experiments. Numbers refer to the durations of each stage in minutes.

Results

Quasi-hydrostatic transformation in the ringwoodite stability field

The experimental conditions and results are summarised in Table 1. All samples were partially transformed after the experiments except samples Ol31 and Ol36, which were held at temperatures too low to induce transformation (600° and 800°C). The dislocation density (10^{11} m^{-2}) of the unreacted olivine single crystal in sample Ol31 (after pressurisation to 18 GPa) was determined in order to constrain the differential stress in the quasi-hydrostatic multianvil sample assembly at 18 GPa prior to transformation. Based on the dislocation density versus stress calibration of Kohlstedt *et al.* (1976) the differential stress ($\sigma_1 - \sigma_3$) is estimated to be ~30 MPa prior to reaction.

In the initial stages of reaction, isolated grains of ringwoodite nucleate incoherently on grain boundaries in the fine-grained olivine matrix (Fig. 5*a*). With increasing time, nucleation saturates the grain boundaries and the olivine single crystals as well as the smaller grains of the matrix become surrounded by polycrystalline reaction rims (Fig. 5*b*). These rims, which consist of a mixture of ringwoodite and wadsleyite, broaden with time. No compositional differences have been detected between the reactant and product phases using analytical transmission electron microscopy (ATEM), thus suggesting that the growth of the product phases is interface-controlled. The growth rates of the reaction rims have been estimated by

TABLE 1. Summary of experimental conditions and results

Sample no.	Pressure (GPa)	Temperature (°C)	Reaction time (min)	Phases present	Rim thickness (μm)	Intratrystalline α−γ transformation
Ol 131	18	600	30	α	0	none
Ol 36	18	800	1380	α	0	none
Ol 40	18	900	300	α, γ	4±2	α→γ
Ol 38	18	900	600	α, β, γ	6±2	α→γ
Ol 33	18	900	900	α, β, γ	6±4	α→γ
Ol 25	18	1000	300	α, β, γ	22±2	α→γ
Ol 32	18	1100	20	α, β, γ	12±2	α→γ
Ol 22	18	1100	60	α, β, γ	22±2	α→γ
Ol 24	18	1100	240	α, β, γ	22±2	α→γ
Ol 30	18	1400	30	β	20?[1]	?[2]
Ol 26	19	1100	60	α, β, γ	20±2	α→γ
Ol 27	20	1100	60	α, β, γ	12±2	α→γ
EQ 6	15	900	30	α, β	—	—
EQ 5	16	900	660	α, β, γ	—	—

[1] rim not clearly identifiable
[2] there might have been some intracrystalline transformation before the whole crystal transformed to wadsleyite

dividing their widths by the reaction time (assuming that product grains nucleated rapidly as soon as the transformation conditions were reached). For longer reaction times, the growth rates do not remain constant, but decrease dramatically with time and growth eventually ceases (Fig. 6*a*). Decreasing growth rates of wadsleyite reaction rims around San Carlos olivine single crystals at lower pressures (13.5–15 GPa) have also been reported by Kubo *et al.* (1998*a,b*). At temperatures $\leqslant$1230°C, they observed growth rates which eventually became zero, as in our experiments. At high temperature (1330°C) however, although the growth rate slowed considerably, it did not become zero (Fig. 6*b*). Whereas impingement of the growing rim with crystals growing in the interior of the olivine single crystal (Fig. 5(b)) may contribute to the cessation of rim growth in our experiments, this cannot explain the decrease in growth rates in the experiments of Kubo *et al.* (1998*a,b*) in which intracrystalline transformation did not occur. We therefore suggest that the decrease in growth rates is caused by the negative volume change (6–8%) during transformation which results in a misfit strain during rim growth. The misfit strain increases with the width of the rim and results in an increase in the stored elastic strain energy. This strain energy, if not dissipated, will decrease the net driving force ΔG for the transformation and eventually stop the transformation. A model for the role of transformation strain is presented below.

In all samples from experiments at $T \geqslant 900$°C intracrystalline transformation occurred in the olivine single crystals and resulted in the formation of numerous optically-visible lenses of wadsleyite (Fig. 5*b*, Table 1). TEM investigations reveal that in addition to wadsleyite, ringwoodite is also present in olivine. Ringwoodite nucleates at intracrystalline sites in olivine (Table 1) and occurs as numerous plate-like lamellae, tens of nm wide and from tens of nm to a few μm long, which are oriented parallel to $(100)_\alpha$ (Fig. 7*a*). These ringwoodite lamellae are crystallographically oriented with respect to olivine such that the close-packed planes $(100)_\alpha$ and $\{111\}_\gamma$ are parallel and the directions $[001]_\alpha$ and $<110>_\gamma$ are collinear. The lamellae have been found only in the interior of the large olivine single crystals and not in the fine-grained matrix grains. The lamellae appear to nucleate throughout the entire volume of the single crystals with a slight tendency toward clustering. Regions with higher densities of lamellae also contain higher densities of dislocations.

High resolution transmission electron microscopy (HRTEM) was used to investigate the morphology of the ringwoodite lamellae and the α–γ interfaces in detail (Fig. 7*b* and *c*). The

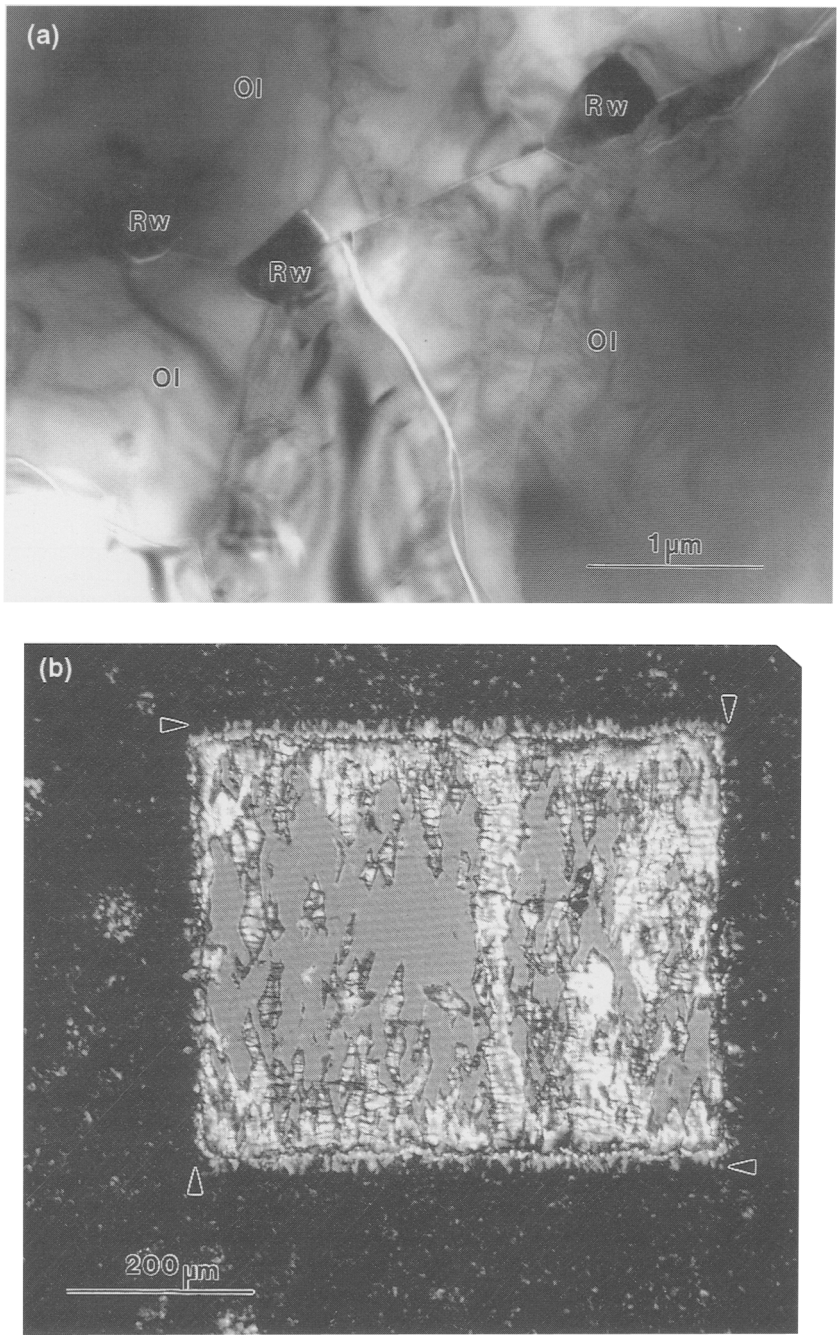

FIG. 5. (*a*) TEM bright field image showing the initial stage of transformation by incoherent grain boundary nucleation and growth. Nuclei of ringwoodite (Rw) form on olivine (Ol) grain boundaries and triple junctions. (*b*) Optical micrograph (crossed nicols) of a partly-reacted olivine single crystal (Ol) in sample Ol26 viewed along the *c*-direction, showing a reaction rim which has formed at the margins of the crystal (arrowheads). In the interior of the single crystal many wadsleyite lenses are visible.

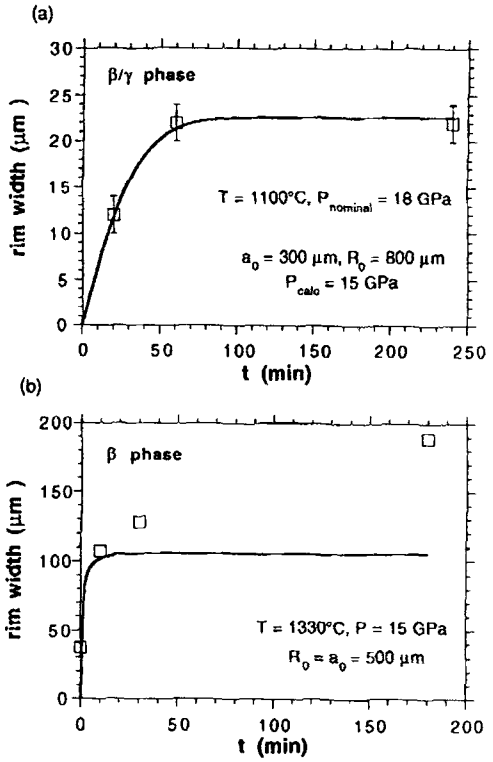

FIG. 6. Comparison of the experimentally-determined and calculated reaction rim widths as a function of reaction time. (*a*) Fit to our data obtained at 18 GPa and 1100°C. In order to obtain this good fit, it was necessary to use a starting pressure of 15 GPa rather than 18 GPa. This is because the fine-grained olivine matrix surrounding the olivine single crystal transforms first and results in a pressure drop due to the negative volume change (see discussion of 5.2). The fit suggests that by the time the transformation in the matrix is near completion, the confining pressure in the sample assembly has decreased by about 3 GPa. The external boundary R_0 (see below) is assumed to be 800 μm to be consistent with the 1.6 mm diameter of the experimental samples. a_0 = 300 μm is taken as the average radius of the single crystal (500 × 600 × 700 μm). (*b*) Growth rates of wadsleyite reaction rims at 1330°C and 15 GPa from Kubo *et al.* (1998*a*,*b*). In their multianvil experiments, single crystals of San Carlos olivine with an edge length of 1 mm were contained in a NaCl confining medium. Because in this case there is no volume decrease in the matrix phase, we assume that the confining pressure remained unchanged during the experiment and $R_0 = a_0$ = 500 μm for our calculation (modified from Liu *et al.*, 1998). The poor fit at long reaction times is due to viscoelastic relaxation which occurs because of the relatively high temperature.

lamellae generally have rounded ends although in detail the interfaces are stepped and show many ledges of unit-cell dimensions (Fig. 7*b* and *c*). Commonly, $\{110\}_\gamma$ stacking faults occur within the lamellae. Some twinned ringwoodite lamellae with a coherent twinning plane in $\{111\}_\gamma$ have been observed (Fig. 7*b*). Many lamellae are associated with planar defects in the olivine structure which normally extend beyond the ends of the lamellae and commonly occur in pairs (Fig. 7*b*). Diffraction contrast experiments revealed that these defects are terminated by partial dislocations and are therefore $(100)_\alpha$ stacking faults. The microstructural relationships and the morphology of the lamellae suggest that ringwoodite nucleates on previously-formed $(100)_\alpha$ stacking faults and then grows by the lateral migration of the ledges which are present at the interphase boundaries. Analytical TEM measurements show no compositional differences between the ringwoodite lamellae and the host olivine which suggests that the growth of the lamellae is not controlled by long-range diffusion and could be interface-controlled.

The optically-visible lenses in the single crystals consist mainly of wadsleyite (Fig. 5*b*). TEM reveals that these lenses are always associated with the ringwoodite lamellae, and it appears that the latter acted as nucleation sites for the wadsleyite lenses (Fig. 8). The small wadsleyite lenses are monocrystalline, whereas the larger, optically visible wadsleyite lenses are polycrystalline and appear to consist of randomly oriented grains. The wadsleyite lenses lie essentially parallel to the {101} planes of olivine (Fig. 8). Our current interpretation of these observations is that wadsleyite grains nucleate on ringwoodite lamellae, probably at the interphase boundary with olivine, as soon as the local transformation strain becomes sufficiently high to stabilise this phase (see below). This interpretation is supported by the observation that wadsleyite always forms on the thickest ringwoodite lamellae. Further wadsleyite grains appear to nucleate incoherently at the α−γ and α−β interfaces to form the optically visible lenses. However, the details of this process remain to be investigated in detail.

Non-hydrostatic transformation in the wadsleyite + ringwoodite stability field

Two samples were pressurised at 900°C to 15 and 16 GPa following hot-pressing and then held at

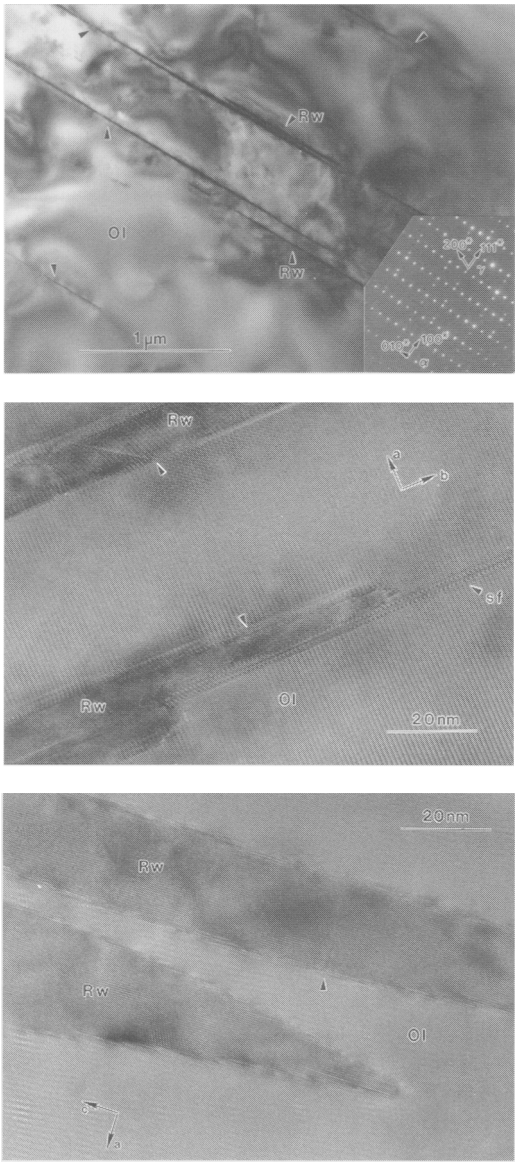

FIG. 7. (*a*) TEM bright field image of thin ringwoodite lamellae (Rw) in host olivine (Ol). The inset shows an electron diffraction pattern of the $[001]_\alpha$ and $<110>_\gamma$ zone axes which illustrates the crystallographic orientation relationship $[100]^*_\alpha // <111>^*_\gamma$. (*b*) HRTEM image of ringwoodite lamellae (Rw) in host olivine (Ol) as viewed along the *c* axis of olivine, with a pair of $(100)_\alpha$ stacking faults (sf) extending out of a twinned ringwoodite lamella and the two halves of the twinned lamella growing along the two faults. Arrows indicate the crystallographic orientation of the olivine. The rounded ends of the lamellae and several $\{110\}_\gamma$ stacking faults (arrow heads) are visible. (*c*) HRTEM image of two ringwoodite lamellae as viewed along the b axis of olivine. Notice the stepped interfaces in (*b*) and (*c*).

these conditions for 30 min and 11 h respectively (Table 1). Because the olivine sample extends for almost the entire length of the sample assembly in these experiments (Fig. 3*b*), the temperature variation along the samples was very large. At the ends of the sample, where the temperature was lowest, olivine failed to transform (cf. Brearley *et al.*, 1992). In the vicinity of the thermocouple junction, where the temperature was highest (900°C), transformation to wadsleyite was about 70% complete in the experiment at 15 GPa and almost 100% complete after 11 h at 16 GPa.

Relict olivine grains in the short-duration 15 GPa experiment are frequently lens-shaped, with high aspect ratios, and are oriented with their short axis approximately parallel to the long axis of the cylindrical sample. The reaction rims which have partially or totally consumed these lens-shaped relics consist of elongate 'fingers' of wadsleyite which are oriented parallel to the same direction (Fig. 9*a*). This texture indicates that the transformation of olivine has occurred under conditions of non-hydrostatic stress with the direction of the principal compressive stress being approximately parallel to the long axis of the cylindrical sample (Vaughan *et al.*, 1984; Green *et al.*, 1992). Non-hydrostatic stress develops because of the anisotropic elastic properties of the sample assembly which result from combining a long sample with the dense-aluminum piston (Fig. 3*b*), i.e. the sample + piston combination is stiffer than the MgO pressure medium. As shown in Fig. 9*b*, the wadsleyite grains in this sample contain a high density of $(010)_\beta$ stacking faults (which extend across entire grains) but a low density of dislocations ($< 3 \times 10^{12}$ m^{-2}); in contrast the dislocation density in the relict olivine grains is very high.

In the longer (11 h) 16 GPa experiment, the wadsleyite grains contain mostly b=[100] dislocations in a configuration indicative of climb (dislocation density $\leqslant 10^{13}$ m^{-2}). Compared with the shorter experiment, the density of $(010)_\beta$ stacking faults is relatively low, which suggests that these defects anneal out with time (as suggested by Brearley *et al.*, 1992).

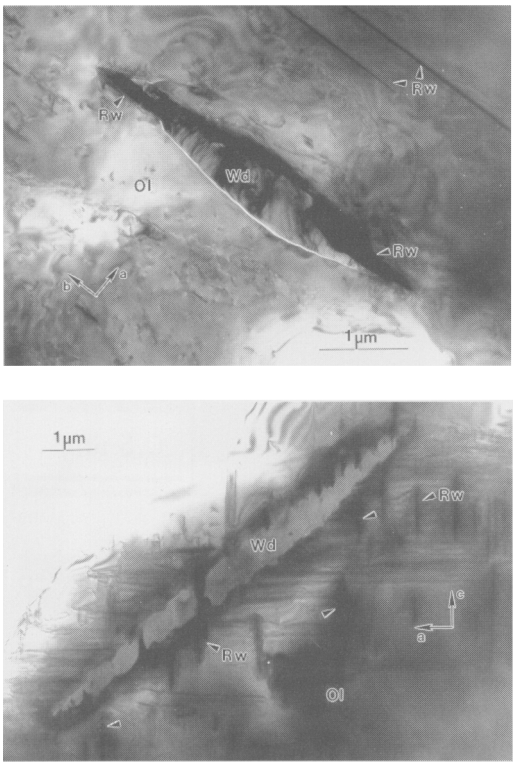

FIG. 8. (*a*) TEM bright field image of an incoherent wadsleyite lens (Wd) oriented along the **b** direction of olivine (Ol). The two dark areas at the tips of this lens consist of ringwoodite (Rw), which is coherent with the olivine. Two ringwoodite lamellae are also visible at the upper right corner of the image. (*b*) Bright field image of another wadsleyite lens (Wd) lying parallel $(101)_\alpha$. Several ringwoodite lamellae (Rw) are also visible, some of them cutting through the wadsleyite lens.

Numerous disk-shaped inclusions of ringwoodite (100–500 nm in diameter and ~50 nm thick) are present at intracrystalline sites in wadsleyite from this experiment. Distinctive arrays of inclusions lie along b = [100] dislocations (Fig. 9*c,d*). The ringwoodite inclusions are crystallographically oriented with respect to wadsleyite such that $(100)_\beta//\{1\bar{1}0\}_\gamma$, $(010)_\beta//\{110\}_\gamma$ and $(001)_\beta//\{001\}_\gamma$. As these inclusions grow in thickness, they coalesce to form long ellipsoidal-shaped grains (Fig. 9*c*). In some cases it can be seen that the disks lie on $(010)_\beta$ stacking faults and have nucleated where these stacking faults intersect the **b** = [100] dislocations. Although in many cases stacking faults are not present, the spacing of the ringwoodite disks is comparable to the spacing of stacking faults in the shorter 30 min experiment (cf. Fig. 9*b,c*). We therefore believe that the disks nucleated, in general, at the intersections of stacking faults and dislocations and that the stacking faults have subsequently annealed out. Because differential stress controls the density of dislocations, the rate of intracrystalline nucleation of ringwoodite in wadsleyite by this mechanism must be stress-dependent. Stress will thus enhance the kinetics of the $\beta \rightarrow \gamma$ transformation.

ATEM analyses of wadsleyite and the disk-shaped ringwoodite inclusions in the 16 GPa experiment indicate that these phases have significantly different iron contents and possibly also slightly different Si contents (see also Hazen *et al.*, 1993). Wadsleyite analyses obtained from areas distant from the inclusions have almost the same mean composition as the San Carlos olivine starting material, $Mg_{1.81}Fe_{0.19}Ni_{0.01}Si_{1.00}O_4$ (Fe/(Fe+Mg) = 10%). In contrast, the mean composition of the ringwoodite inclusions is $Mg_{1.63}Fe_{0.30}Ni_{0.01}Si_{1.03}O_4$ (Fe/(Fe+Mg) = 16%). These different chemical compositions are consistent with the ringwoodite forming in the two-phase $\beta + \gamma$ stability field and suggest that the growth of this phase is diffusion-controlled in this case. It is possible that the growth rate is enhanced by the dislocations because diffusion is faster along dislocation lines (pipe diffusion) than through defect-free crystals.

Discussion

Intracrystalline nucleation mechanisms

We have observed two types of intracrystalline nucleation during the $\alpha-\beta-\gamma$ transformations: (i) intracrystalline nucleation of ringwoodite in olivine and (ii) intracrystalline nucleation of ringwoodite in wadsleyite. The formation of wadsleyite in the interior of olivine single crystals (Fig. 5*b*) cannot be termed intracrystalline because this phase appears to have nucleated at olivine–ringwoodite interfaces. Although intracrystalline $\alpha \rightarrow \gamma$ transformation was first observed more than 10 years ago, it has only recently been shown to operate at geologically-realistic differential stress levels (Burnley, 1995; Kerschhofer *et al.*, 1996). Liu and Yund (1995) suggested that intracrystalline transformation rates may be comparable to the rate of grain boundary nucleated transformation in subduction zones. However, no detailed studies of the

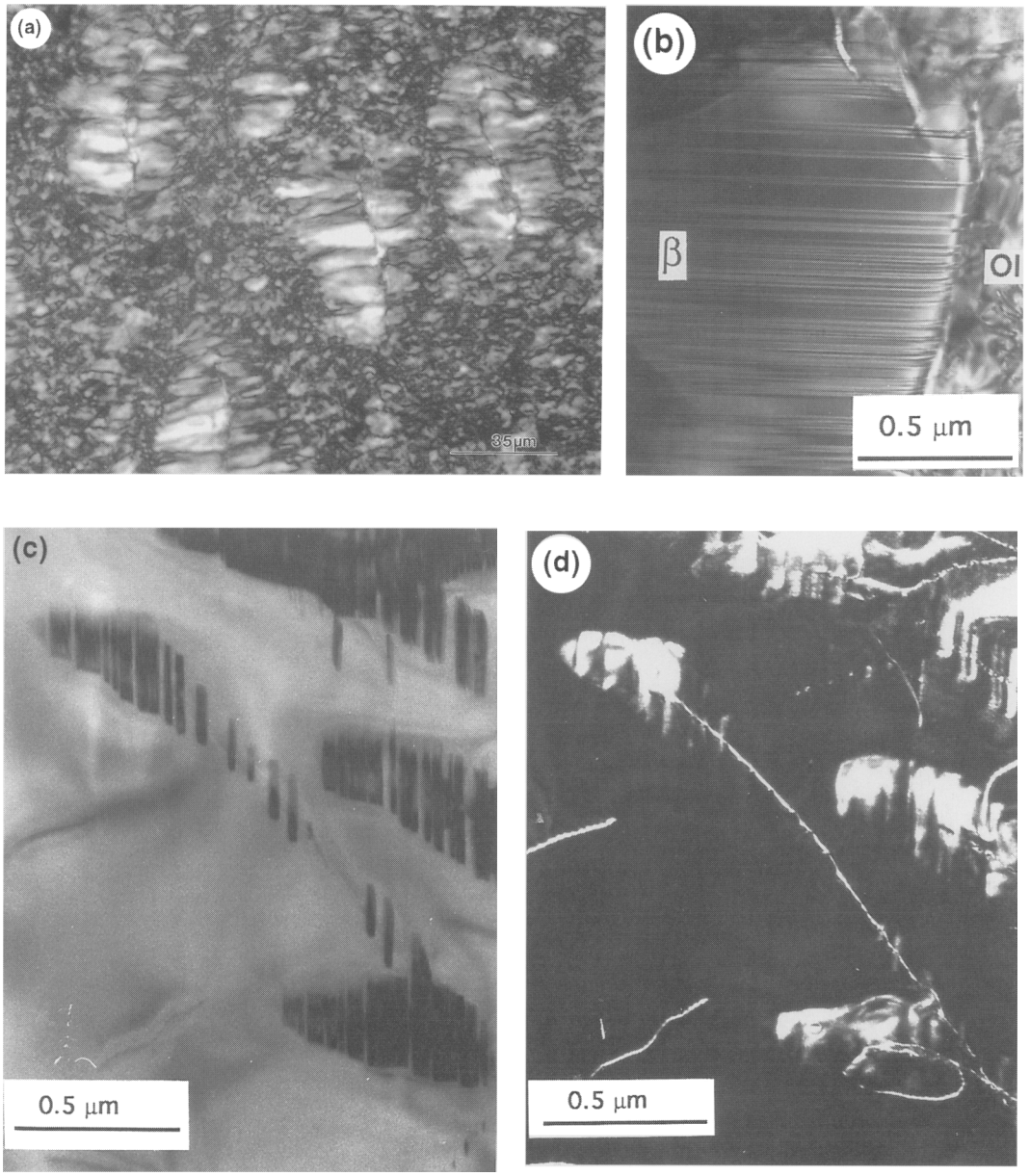

FIG. 9. (*a*) Optical micrograph showing lens-shaped pseudomorphs after olivine elongated perpendicular to the direction of principal compressive stress (sample EQ5). Elongate wadsleyite grains that nucleated at olivine grain boundaries grew parallel to the principal compressive stress to consume the olivine grains. (*b*) TEM bright field image of straight (010) stacking faults in the elongated β-phase grains. (*c*) Bright field image of disk-shaped inclusions of ringwoodite (dark) in a host wadsleyite grain. The long dimension of these inclusions is parallel to $(010)_\beta$. (*d*) TEM weak beam image of **b** = [100] dislocations in the same area as in (*c*). It is clear that the ringwoodite inclusions have nucleated on these dislocations.

morphological and kinetic details of this mechanism have been conducted previously.

It has generally been assumed that γ-phase lamellae at intracrystalline sites in olivine with the orientation relationship $(100)_\alpha//\{111\}_\gamma$ are strong indications for the martensitic transformation mechanism predicted by Poirier (1981) and that the presence of $(100)_\alpha$ stacking faults, in addition, would be proof of this mechanism. For the first time we have found $(100)_\alpha$ stacking faults in partly-reacted olivine single crystals. However, the morphology of the ringwoodite lamellae in our samples differs considerably from that of true martensitic products in metals, where the coherent product phase lamellae are characterised by pointed ends and an extremely high density of stacking faults (Nishiyama, 1978). In contrast, the lamellae found in our samples have rounded ends and moderate $\{110\}_\gamma$ stacking fault densities. The lengths and thicknesses of the γ-phase lamellae in our samples (Fig. 7*a*) indicate that growth is slow, even for the initial layer of γ-phase, which is untypical for martensitic transformations (Nishiyama, 1978). Furthermore, intracrystalline $\alpha \rightarrow \gamma$ transformation in our experiments appears to be thermally activated, because at high pressure (18 GPa) and low temperatures (600°C and 800°C) the formation of ringwoodite lamellae has not been observed. Growth of the lamellae appears to proceed by the lateral migration of ledges (Fig. 7*b,c*). We therefore conclude that the intracrystalline $\alpha \rightarrow \gamma$ transformation proceeds by the coherent nucleation of ringwoodite on previously formed $(100)_\alpha$ stacking faults and growth is likely to be interface-controlled. This mechanism is completely different from a martensitic process.

As mentioned above, it had been concluded previously that intracrystalline $\alpha \rightarrow \gamma$ transformation only occurs at high differential stresses (e.g. >1 GPa, Burnley and Green, 1989). High stresses would be necessary if the intracrystalline transformation occurs by the shear-induced coordinated movement of atoms. However, based on observed dislocation densities in olivine prior to transformation, the coherent ringwoodite lamellae formed in our samples at differential stresses much lower than 1 GPa. Intracrystalline $\alpha \rightarrow \gamma$ transformation is therefore not restricted to conditions of high differential stress (at least in natural silicate systems), but can occur over a wide range of differential stresses (e.g. compare our results with those of Madon *et al.*, 1989).

Burnley (1995) proposed that a large pressure overstep is necessary to induce the intracrystalline $\alpha \rightarrow \gamma$ transformation because of the large change in free energy. However, the pressure oversteps in her study (8–14 GPa) were considerably larger than those of our experiments (ΔP = 4–5 GPa relative to the metastable α–γ phase boundary — see Kerschhofer *et al.*, 1996). Therefore, at least in natural olivine, the necessary pressure overstep is not as large as previously suggested.

In our samples we have observed intracrystalline $\alpha \rightarrow \gamma$ transformation only in the large olivine single crystals and not in the fine-grained matrix, suggesting that intracrystalline nucleation of ringwoodite is dependent on the olivine grain size. Although grain size dependence of intracrystalline transformation of olivine has not been proposed previously, results from most previous experimental studies are consistent with this hypothesis. In studies which have reported evidence for intracrystalline transformation under low differential stresses, starting materials with grain sizes of 80 μm (Burnley, 1995) or even a few mm (Hamaya and Akimoto, 1982) have been used. On the other hand, experiments performed on fine-grained starting materials, e.g. 30 μm (Rubie and Champness, 1987) and 1–5 μm (Boland and Liebermann, 1983), at moderate differential stresses only resulted in transformation by incoherent grain boundary nucleation and growth. Martinez *et al.* (1997) observed intracrystalline ringwoodite lamellae in ~150 μm San Carlos olivine single crystals reacted at 1200°C and 26 GPa in a multianvil apparatus whereas only grain boundary nucleation and growth was observed when fine-grained olivine (10–20 μm) was reacted at the same conditions. Intracrystalline transformation was not reported in two studies on Co_2SiO_4 olivine in which the grain size was 100–300 μm, but in these cases the pressure overstep was very small (Remsberg *et al.*, 1988; Remsberg and Liebermann, 1991). In diamond anvil cell experiments however, in which differential stresses were very high, intracrystalline transformation has been observed in olivine that was presumably fine-grained (e.g. Boland and Liu, 1983; Madon *et al.*, 1989). The reason for intracrystalline $\alpha \rightarrow \gamma$ transformation occurring preferentially in coarse-grained samples may be due to thermal stresses which develop during heating because the magnitude of such stresses increases with grain-size for anisotropic minerals such as olivine (Cleveland and Bradt, 1978). Furthermore, the development of strain

energy caused by the growth of grain-boundary nucleated reaction rims may also play a role (Liu *et al.*, 1998).

The conclusion from this discussion is that intracrystalline transformation is enhanced by differential stress that develops during transformation and probably also by the extent of pressure overstep. The specific role of differential stress may be to induce (or enhance) formation of the $(100)_\alpha$ stacking faults which act as the nucleation sites for γ-phase lamellae.

The topotaxial relations between ringwoodite and wadsleyite found in sample EQ5 have already been found in natural materials from shock-produced veins in chondritic meteorites (Price *et al.*, 1982; Price, 1983; Madon and Poirier, 1983) and in other experimental studies performed under conditions of quasi-hydrostatic stress (Brearley *et al.*, 1992; Brearley and Rubie, 1994; Rubie and Brearley, 1990, 1994). However, in these experimental studies, grain boundary nucleation was the dominant mechanism during the $\beta \rightarrow \gamma$ transformation and intracrystalline nucleation of ringwoodite within host wadsleyite grains has not been reported previously. The fault-like intergrowths in shocked meteorites may form by a phase transformation involving shear (Madon and Poirier, 1983) or, alternatively, might be growth defects. The ringwoodite inclusions found in our samples have a disk-like form and chemical compositions different from that of the host wadsleyite, which probably rules out their formation by a shear mechanism involving the migration of partial dislocations. The nucleation of these inclusions is obviously correlated with the presence of dislocations and probably occurs where such defects intersect stacking faults. These findings demonstrate that intracrystalline nucleation of ringwoodite in wadsleyite is enhanced by differential stress, because this variable determines the dislocation density.

The enhancement of transformation kinetics by differential stress has been documented by Wu *et al.* (1993) from the results of *in situ* X-ray diffraction experiments of the $\alpha \rightarrow \beta$ and $\alpha \rightarrow \gamma$ transformations in the diamond anvil cell (in the compositions Fe_2SiO_4 and Mg_2SiO_4). However, these authors did not investigate the mechanisms by which stress enhanced the kinetics during these transformations. For the olivine–ringwoodite and wadsleyite–ringwoodite transformations discussed in this paper, we conclude that the kinetics are likely to be enhanced by differential stress through the creation of new intracrystalline nucleation sites.

Role of transformation strain

Because the molar volumes of the α-, β- and γ-phases differ significantly from each other, strain will always be generated during the $\alpha-\beta-\gamma$ phase transformations. The significance of transformation strain for kinetic models lies in its effect on the growth rates of the product phase. As discussed above, we propose that the time-dependent growth rate for an incoherently nucleated reaction rim (Fig. 5*b*) is due to the increasing elastic strain associated with the phase transformations. Here, assuming pure elasticity, we use a simple model (Fig. 10*a*) to offer a quantitative explanation (details can be found in Liu *et al.*, 1998). The term spinel is used here to denote β- or γ-phase. Consider that a spherical olivine inclusion is embedded in a finite spinel matrix of radius R_0 and is gradually consumed by the growth of a spinel reaction rim. The spinel matrix is derived by rapid transformation of the fine-grained olivine which originally surrounded the olivine single crystal. The spherical geometry is adopted for mathematical convenience. Because of the negative volume change associated with the transformation, there exists a misfit strain (ε) in the olivine inclusion. In other words, if the olivine inclusion was unconstrained, there would be a gap between the inclusion and the spinel matrix (Fig. 10*b*). The radii of the inclusion and the spherical hole in the matrix would be $a(1 + \varepsilon)$ and a, respectively. This misfit strain ε is given by:

$$\varepsilon = \frac{a_0^3 - a^3}{3a^3} \frac{\Delta V_{sp-ol}}{V_{ol}} \tag{4}$$

where V is molar volume, and a_0 is the inclusion radius at time $t = 0$.

When the inclusion with a misfitting strain ε is constrained by the matrix, elastic strains and consequently elastic strain energy will develop in the system. The stresses and strains in the system can be obtained by applying displacement continuity, mechanical equilibrium and given boundary conditions to the standard solution for a misfitting inclusion problem (Liu *et al.*, 1998 and references therein). If we assume that the outer surface of the matrix R_0 is subject to a constant pressure P, the solution leads to the strain energy in the system (Liu *et al.*, 1998):

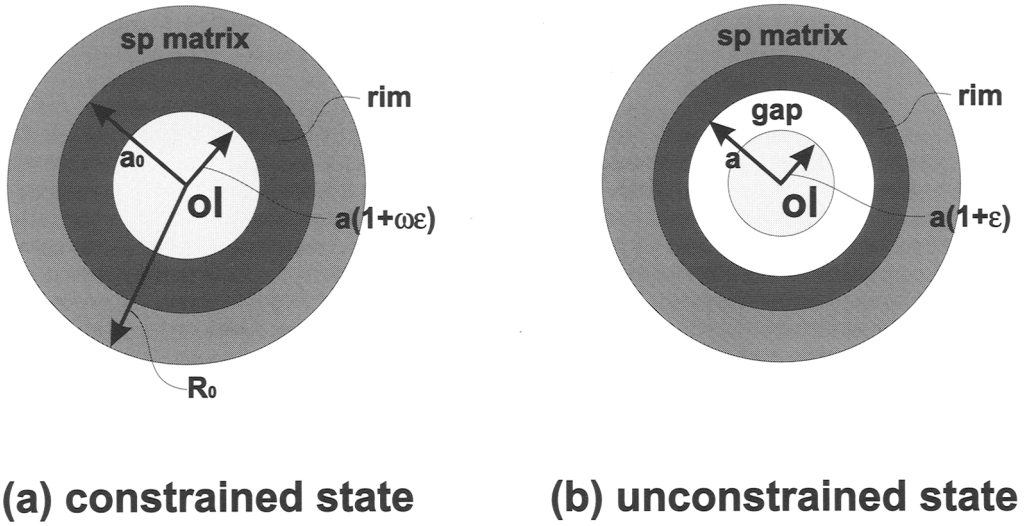

FIG. 10. A simplified geometry for a spinel reaction rim surrounding a misfitting olivine inclusion, which initially had a radius a_0 and was embedded in a spinel matrix of radius R_0. (*a*) The inclusion in a constrained state has an effective radius $a(1 + \omega\varepsilon)$, where ω is a numerical factor to be determined (see text). (*b*) In a stress-free state (unconstrained), there is a misfit (gap) between the inclusion of radius $a(1+ \varepsilon)$ and the spherical hole of radius a within the matrix (modified from Liu *et al.*, 1997).

$$W_{el} = 6\pi[a^3 K_{ol}(\omega - 1)^2\varepsilon^2 + \left(K_{sp}C_1^2 + \frac{4\mu_{sp}C_2^2}{3R_0^3a^3}\right)(R_0^3 - a^3)] \quad (5)$$

where K and μ are bulk and shear moduli respectively, $C_1 = 4\mu_{sp}\omega\varepsilon a^3/(3K_{sp}R_0^3 + 4\mu_{sp}a^3)$, $C_2 = 3K_{sp}\omega\varepsilon a^3R_0^3/(3K_{sp}R_0^3 + 4\mu_{sp}a^3)$, and

$$\omega = \frac{K_{ol}}{K_{ol}+\tau\mu_{sp}} \text{ with } \tau = \frac{4K_{sp}(R_0^3-a^3)}{3K_{sp}R_0^3+4\mu_{sp}a^3}.$$

Thus, if the contribution of interfacial energy is small and can be ignored, the total Gibbs energy change of the system during the growth of the spinel reaction rim is:

$$\Delta G = \tfrac{4}{3}\pi(a_0^3 - a^3)\Delta G_V^{sp-ol}(P) + W_{el} \quad (6)$$

where $\Delta G_V^{sp-ol}(P)$ is the chemical free energy change for a unit volume of olivine transformed to spinel at the hydrostatic stress P.

Because the magnitude of ε increases as the rim grows (Equation (4)), W_{el} will also increase with time. This causes $\Delta G \rightarrow 0$ and eventually stops the rim growth if the transformation strain is not relaxed by viscoelastic flow. Liu *et al.* (1997) modified Rubie and Ross's (1994) equation for interface-controlled growth by taking non-hydrostatic stress and elastic strain energy into account. They calculated the width of the reaction rim as a function of time. The results are compared with our experimental data (Fig. 6*a*) and those of Kubo *et al.* (1998*a,b*) (Fig. 6*b*). The good agreement between the calculation and our experimental observations shown in Fig. 6*a* is consistent with the hypothesis that transformation strain plays an important role in controlling the growth rate of grain-boundary nucleated reaction rims. In addition, Fig. 6*a* suggests that viscoelastic relaxation of the elastic strain is negligible for $T \leqslant 1100°C$ on a laboratory time scale. At higher temperatures, viscoelastic relaxation evidently allows the rim to continue growing but at a considerably slower rate than at the beginning of the experiment when the strain energy is zero (Fig. 6*b*). In subduction zones, where the time scale is much longer than in our experiments, viscoelastic relaxation is inevitable, even though the temperatures are lower, and the transformation kinetics for grain boundary nucleated reaction rims may be controlled to a large extent by this process. This conclusion highlights the problem of extrapolating experimentally-determined growth rates to geological conditions. However, with reference to an analogous situation, it should

also be noted that large pressure differences (e.g. 0.7 GPa at 800°C) can persist between mineral inclusions in strong phases such as garnet and the externally-applied pressure, even on geological time scales (e.g. Gillet *et al.*, 1984; Darling *et al.*, 1997).

Evolution of pressure

Our quasi-hydrostatic experiments were performed at a nominal pressure of 18–20 GPa, in the ringwoodite stability field (Fig. 4). The fact that ringwoodite is the dominant phase at early stages of transformation (Fig. 5*a*) is therefore consistent with the pressure calibration. However, as transformation proceeds, wadsleyite becomes the dominant product phase (see Fig. 8, Table 1). The formation of wadsleyite is likely to be a consequence of transformation strain which can cause a significant localised pressure drop (Liu *et al.*, 1998). An additional factor could be the hot-pressing stage which might reduce the final pressure relative to that estimated from the calibration.

In situ X-ray diffraction studies of high-pressure phase transformations, performed in multianvil apparatus, have documented significant drops in pressure in the sample assembly (up to 2–3 GPa) as a consequence of the decrease in the sample volume (E. Ohtani, pers. comm.). Maintaining the hydraulic oil pressure of the multianvil press at a constant value evidently does not compensate for the reduction in sample volume because of the strength of the pressure medium and gaskets. This phenomenon might also explain why wadsleyite is a common transformation product in our experiments at the nominal pressures of 18–20 GPa. It also explains why it was necessary to adopt a starting pressure of 15 GPa in the strain energy model described above (Fig. 6*a*) — this is effectively the pressure after transformation of the fine-grained olivine matrix. Such pressure reduction during phase transformations, which is clearly a significant problem for a range of kinetic, phase equilibria and pressure-calibration experiments, can probably be minimised by keeping the size of the sample as small as possible.

Competing transformation mechanisms

We have observed that large olivine crystals transform at high pressure by two mechanisms, involving incoherent grain boundary nucleation and coherent intracrystalline nucleation respectively (Fig. 11). These mechanisms obviously compete with each other, as suggested by Liu and Yund (1995). The two mechanisms must also interact, probably in at least two ways. First, the development of wadsleyite crystals in the interior of olivine grains will inhibit growth of grain-boundary nucleated reaction rims (even without considering the strain energy effect discussed above). Second, the strain produced by growth of the grain-boundary nucleated reaction rims may result in non-hydrostatic stresses which enhance the kinetics of intracrystalline nucleation. These two interactions combined will result in product phases with a grain size that is small compared with that expected from transformation by grain boundary nucleation alone (Fig. 11). Such complexities should be taken into account when predicting changes in rheology due to grain size reduction during polymorphic phase transformations (e.g. Rubie, 1984, 1990; Riedel and Karato, 1996, 1997).

Conclusion

A major aim of experimental studies of the transformation of olivine to the high-pressure polymorphs wadsleyite and ringwoodite has been to obtain kinetic data which can be extrapolated to subduction zone conditions. In this paper we have documented new complexities that must be taken into account when extrapolating kinetic data. First, our results show that intracrystalline transformation occurs in laboratory experiments at moderate differential stresses and is therefore probably also important in subduction zones. Thus, it is important to quantify the kinetics of this mechanism. Second, our results show that transformation strain, that develops during transformation because of the different densities of the three polymorphs, plays an important role because it can reduce growth rates to zero at an early stage of transformation on short time scales. Under geological conditions, growth rates may be controlled by viscoelastic relaxation. Furthermore, differential stress will enhance the kinetics of the $\beta \rightarrow \gamma$ transformation by generating dislocations which act as intracrystalline nucleation sites. Stress may also play a comparable role during intracrystalline $\alpha \rightarrow \gamma$ transformation. Even if there is no externally applied stress, non-hydrostatic stresses will always develop in a transforming polycrystalline aggregate because of the effect of temperature and

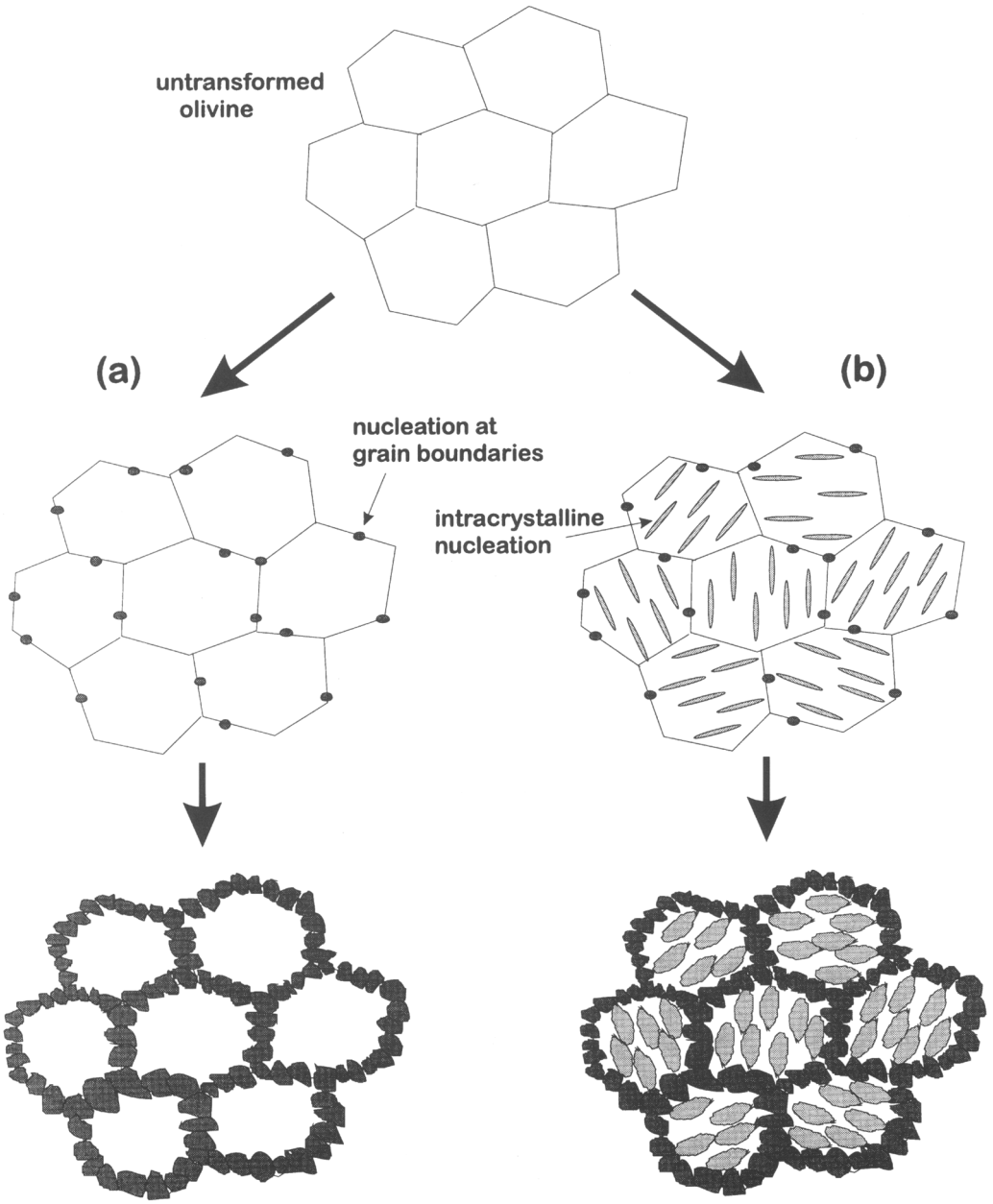

FIG. 11. Possible evolution of microstructure (*a*) if olivine transforms by grain boundary nucleation and growth alone, and (*b*) if olivine transforms by grain boundary nucleation and intracrystalline nucleation mechanisms simultaneously.

the effect of transformation strain. The role of differential stress needs to be further evaluated and eventually incorporated into kinetic models.

Acknowledgements

We thank S. Karato, J.D.C. McConnell and F. Seifert for helpful discussions, R. Miletich for his help with the orientation of the olivine single crystals and H. Küfner and H. Schulze for technical support and sample preparation. We are grateful for financial support by the Deutscher Akademischer Austauschdienst (A/95/09994), the EU "Training and Mobility of Researchers" Programme (Contract No. ERBFMBICT960758), the EU "Human Capital and Mobility - Access to Large Scale Facilities" Programme (Contract No. ERBCHGECT940053), the alexander von Humboldt Foundation and the National Science Foundation (Grant EAR-9627863).

References

Akaogi, M., Ito, E. and Navrotsky, A. (1989) Olivine-modified spinel–spinel transitions in the system Mg_2SiO_4–Fe_2SiO_4: Calorimetric measurements, thermodynamical calculation, and geophysical application. *J. Geophys. Res.*, **94**, 15671–85.

Boland, J.N. and Liebermann, R.C. (1983) Mechanism of the olivine to spinel phase transformation in Ni_2SiO_4. *Geophys. Res. Lett.*, **10**, 87–90.

Boland, J.N. and Liu, L. (1983) Olivine to spinel transformation in Mg_2SiO_4 via faulted structures. *Nature*, **303**, 233–5.

Brearley, A.J. and Rubie, D.C. (1994) Transformation mechanisms of San Carlos olivine to $(Mg, Fe)_2SiO_4$ β-phase under subduction zone conditions. *Phys. Earth Planet. Int.*, **86**, 45–67.

Brearley, A.J., Rubie, D.C. and Ito, E. (1992) Mechanisms of the transformations between the α, β and γ polymorphs of Mg_2SiO_4 at 15 GPa. *Phys. Chem. Mineral.*, **18**, 343–58.

Burnley, P.C. (1990) *The effect of nonhydrostatic stress on the olivine-spinel transformation in Mg_2GeO_4.* Thesis, Univ. California, Davies, 187 pp.

Burnley, P.C. (1995) The fate of olivine in subducting slabs: A reconnaissance study. *Amer. Mineral.*, **80**, 1293–1301.

Burnley, P.C. and Green, H.W. II (1989) Stress dependence of the mechanism of the olivine-spinel transformation. *Nature*, **338**, 753–6.

Cahn, J.W. (1956) The kinetics of grain boundary nucleated reactions. *Acta Metall.*, **4**, 449–59.

Canil, D. (1994) Stability of clinopyroxene at pressure-temperature conditions of the transition region. *Phys. Earth Planet. Int.*, **86**, 25–34.

Carlson, W.D. and Rosenfeld, J.L. (1981) Optical determination of topotactic aragonite-calcite growth kinetics: metamorphic implications. *J. Geol.*, **89**, 615–38.

Christian, J.W. (1975) *The Theory of Transformations in Metals and Alloys. I. Equilibrium and General Kinetic Theory*. Pergamon Press, Oxford, 586pp.

Cleveland, J.J. and Bradt, R.C. (1978) Grain size/microcracking relations for pseudobrookite oxides. *J. Amer. Ceram. Soc.*, **61**, 478–81.

Daessler, R., Yuen, D.A., Karato, S. and Riedel, M.R. (1996) Two-dimensional thermo-kinetic model for the olivine-spinel phase transition in subducting slabs. *Phys. Earth Planet. Int.*, **94**, 217–39.

Darling, R.S., Chou, I.-M. and Bodnar, R.J. (1997) An occurrence of metastable cristobalite in high-pressure garnet granulite. *Science*, **276**, 91–3.

Fujino, K. and Irifune, T. (1992) TEM studies on the olivine to modified spinel transformation in Mg_2SiO_4. In *High-Pressure Research: Application to Earth and Planetary Sciences* (Y. Syono and M.H. Manghnani, eds.), Amer. Geophys. Union, Washington D. C., pp. 237–43.

Furnish, M.D. and Bassett, W.A. (1983) Investigation of the mechanism of the olivine-spinel transition in fayalite by synchrotron radiation. *J. Geophys. Res.*, **88**, 10333–41.

Gillet, P., Ingrin, J. and Chopin, C. (1984) Coesite in subducted continental crust: P-T history deduced from an elastic model. *Earth Planet. Sci. Lett.*, **70**, 426–36.

Green, H.W. and Houston, H. (1995) The mechanics of deep earthquakes. *Ann. Rev. Earth Planet. Sci.*, **23**, 169–213.

Green, H.W., Young, T.E., Walker, D. and Scholz, C.H. (1992) The effect of nonhydrostatic stress on the α→β and α→γ olivine phase transformations. In *High Pressure Research: Applications to Earth and Planetary Sciences* (Y. Syono and M.H. Manghnani, eds.), Amer. Geophys. Union, Washington D. C., pp. 229–35.

Goto, K., Suzuki, Z. and Hamguchi, H. (1987) Stress distribution due to olivine-spinel phase transition in descending plate and deep focus earthquakes. *J. Geophys. Res.*, **92**, 13811–20.

Guyot, F., Gwamnesia, G.D. and Liebermann R.C. (1991) An olivine to beta phase transformation mechanism in Mg_2SiO_4. *Geophys. Res. Lett.*, **18**, 89–92.

Hacker, B.R., Kirby, S.H. and Bohlen, S.R. (1992) Time and metamorphic petrology: calcite to aragonite experiments. *Science*, **258**, 110–2.

Hamaya, N. and Akimoto, S. (1982) Experimental investigation of the mechanism of the olivine→spi-

nel transformation: growth of single crystal spinel from single crystal olivine in Ni_2SiO_4. In *High Pressure Research in Geophysics* (S. Akimoto and M.H. Manghnani, eds.), Center Acad. Pub., Tokyo, pp. 373–89.

Hazen, R.M., Downs R.T., Finger, L.W. and Co, J. (1993) Crystal chemistry of ferromagnesian spinels: Evidence for Mg-Si disorder. *Amer. Mineral.*, **78**, 1320–3.

Horiuchi, H., Horioka, K. and Morimoto, N. (1980) Spinelloids: A systematics of spinel-related structures obtained under high-pressure conditions. *J. Mineral. Soc. Japan, Special Issue*, **2**, 253–64.

Horiuchi, H., Akaogi, M. and Sawamoto, H. (1982) Crystal structure studies on spinel-related phases, spinelloids: implications to olivine-spinel phase transformation and systematics. In *Advances in Earth and Planetary Sciences*, **12**, (S. Akimoto and M.H. Manghnani, eds). High Pressure Research in Geophysics, pp. 391–403.

Hornstra, D. (1960) Dislocations, stacking faults and twins in the spinel structure. *J. Phys. Chem. Solids*, **15**, 311–23.

Ito, E. and Katsura, T. (1989) A temperature profile of the mantle transition zone. *Geophys. Res. Lett.*, **16**, 425–8.

Ito, E. and Sato, H. (1991) Aseismicity in the lower mantle by superplasticity of the descending slab. *Nature*, **351**, 140–1.

Karato, S.-I. (1996) Phase transformations and rheological properties of mantle minerals. In *Earth's Deep Interior* (D. Crossley and A.M. Soward, eds.), pp. 223–72.

Katsura, T. and Ito, E. (1989) The system Mg_2SiO_4-Fe_2SiO_4 at high pressures and temperatures: precise determination of stabilities of olivine, modified spinel, and spinel. *J. Geophys. Res.*, **94**, 15663–70.

Kerschhofer, L., Sharp, T.G. and Rubie, D.C. (1996) Intracrystalline transformation of olivine to wadsleyite and ringwoodite under subduction zone conditions. *Science*, **274**, 79–81.

Kirby, S.H., Stein, S., Okal, E.A. and Rubie, D.C. (1996) Metastable mantle phase transformations and deep earthquakes in subducting oceanic lithosphere. *Rev. Geophys.*, **34**, 261–306.

Kohlstedt, D.L., Goetze, C. and Durham, W.B. (1976) Experimental deformation of single crystal olivine with application to flow in the mantle. In *The Physics and Chemistry of Minerals and Rocks* (R.G.J. Strens, ed.), J. Wiley, New York, pp. 35–49.

Kubo, T., Ohtani, E., Kato, T., Shinmei, T. and Fujino, K. (1998*a*) Experimental investigation of the α-β transformation of San Carlos olivine single crystal. *Phys. Chem. Mineral.* (in press).

Kubo, T., Ohtani, E., Kato, T., Shinmei, T. and Fujino, K. (1998*b*) Effects of water on the α–β transformation kinetics in San Carlos olivine. *Science*, **281**, 85–7.

Lacam, A., Madon, M. and Poirier, J.-P. (1980) Olivine glass and spinel formed in a laser heated, diamond-anvil high pressure cell. *Nature*, **289**, 155–7.

Liu, M. and Yund, R.A. (1993) Transformation kinetics of polycrystalline aragonite to calcite: new experimental data, modelling and implications. *Contrib. Mineral. Petrol.*, **114**, 465–78.

Liu, M. and Yund, R.A. (1995) The elastic strain energy associated with the olivine-spinel transformation and its implications. *Phys. Earth Planet. Inter.*, **89**, 177–97.

Liu, M., Kerschhofer, L. and Rubie, D.C. (1998) The effect of strain energy on growth rates during the olivine-spinel transformation. *J. Geophys. Res.* (submitted).

Madon, M. and Poirier, J.-P. (1983) Transmission electron microscope observation of α, β and γ $(Mg,Fe)_2SiO_4$ in shocked meteorites: planar defects and polymorphic transitions. *Phys. Earth Planet. Int.*, **33**, 31–44.

Madon, M., Guyot, F., Peyronneau, J. and Poirier, J.-P. (1989) Electron microscopy of high-pressure phases synthesized from natural olivine in diamond anvil cell. *Phys. Chem. Mineral.*, **16**, 320–30.

Martinez, I., Wang, Y., Guyot, F., Liebermann, R.C. and Doukhan, J.-C. (1997) Microstructures and iron partitioning in $(Mg,Fe)SiO_3$ perovskite - (Mg,Fe)O magnesiowüstite assemblages: an analytical transmission electron microscopy study. *J. Geophys. Res.*, **102**, 5265–80.

Nishiyama, Z. (1978) *Martensitic Transformation* (M.E. Fine, M. Meshii and C.M. Wayman, eds.), Material Science Series, Academic Press, New York, 467pp.

Poirier, J.-P. (1981) Martensitic olivine-spinel transformation and plasticity of the mantle transition zone. In *Anelastic Properties and Related Processes in the Earth's Mantle,* Geodynamic Series, Vol. **4**, Amer. Geophys. Union, Washington D. C., pp. 113–7.

Price, G.D. (1983) The nature and significance of stacking faults in wadsleyite, natural β-$(Mg,Fe)_2SiO_4$ from the Peace River meteorite. *Phys. Earth Planet. Int.*, **33**, 137–47.

Price, G.D., Putnis, A. and Smith, D.G.W. (1982) A spinel to β-phase transformation mechanism in $(Mg,Fe)_2SiO_4$. *Nature*, **296**, 729–31.

Remsberg, A.R. and Liebermann, R.C. (1991) A study of the polymorphic transformation in Co_2SiO_4. *Phys. Chem. Mineral.*, **18**, 161–70.

Remsberg, A.R., Boland, J.N., Gasparik, T. and Liebermann, R.C. (1988) Mechanism of the olivine-spinel transformation in Co_2SiO_4. *Phys. Chem. Mineral.*, **15**, 498–506.

Riedel, M.R. and Karato, S. (1996) Microstructural development during nucleation and growth.

Geophys. J. Int., **125**, 397–414.

Riedel, M.R. and Karato, S. (1997) Grain-size dependence in subducted lithosphere associated with the olivine-spinel transformation and its effect on rheology. *Earth Planet. Sci. Lett.*, **148**, 27–43.

Rubie, D.C. (1983) Reaction-enhanced ductility: the role of solid-solid univariant reactions in deformation of the crust and mantle. *Tectonophysics*, **95**, 331–52.

Rubie, D.C. (1984) The olivine→spinel transformation and the rheology of subducting lithosphere. *Nature*, **308**, 505–8.

Rubie, D.C. (1990) Mechanisms of reaction-enhanced deformability in minerals and rocks. In *Deformation Processes in Minerals, Ceramics and Rocks* (D.J. Barber and P.G. Meredith, eds.), Unwin Hyman, London, pp. 262–95.

Rubie, D.C. (1993) Mechanisms and kinetics of reconstructive phase transformations in the Earth's mantle. In *Short Courses Handbook on Experiments at High Pressure and Applications to the Earth's Mantle* (ed. R.W. Luth), Miner. Assoc. Canada, Vol. **21**, Edmonton, pp. 247–303.

Rubie, D.C. and Brearley, A.J. (1990) Mechanism of the β-γ phase transformation of Mg_2SiO_4 at high temperature and pressure. *Nature*, **348**, 628–31.

Rubie, D.C. and Brearley, A.J. (1994) Phase transitions between β and γ $(Mg,Fe)_2SiO_4$ in the Earth's mantle: mechanisms and rheological implications. *Science*, **264**, 1445–8.

Rubie, D.C. and Champness, P.E. (1987) The evolution of microstructure during the transformation of Mg_2GeO_4 olivine to spinel. *Bull. Mineral.*, **110**, 471–80.

Rubie, D.C. and Ross, C.R. (1994) Kinetics of the olivine-spinel transformation in subducting lithosphere: experimental constraints and implications for deep slab processes. *Phys. Earth Planet. Int.*, **86**, 223–41.

Rubie, D.C. and Thompson A.B. (1985) Kinetics of metamorphic reactions at elevated temperatures and pressures: an appraisal of available experimental data. In *Metamorphic Reactions: Kinetics, Textures and Deformation* (A. B. Thompson and D. C. Rubie, eds.), Advances in Physical Geochemistry **4**, Springer, New York, pp. 27–79.

Rubie, D.C., Tsuchida, Y., Yagi, T., Utsumi, W., Kikegawa, T., Shimonura, O. and Brearley, A.J. (1990) An *in situ* X ray diffraction study of the kinetics of the Ni_2SiO_4 olivine-spinel transformation. *J. Geophys. Res.*, **95**, 15829–44.

Sharp, T.G. and Rubie, D.C. (1995) Catalysis of the olivine to spinel transformation by high clinoenstatite. *Science*, **269**, 1095–8.

Solomatov, V.S. and Stevenson, D.J. (1994) Can sharp seismic discontinuities be caused by non-equilibrium phase transformations? *Earth Planet. Sci. Lett.*, **125**, 267–79.

Sung, C.M. and Burns, R.G. (1976) Kinetics of high-pressure phase transformations: implications to the evolution of the olivine-spinel transition in the downgoing lithosphere and its consequences on the dynamics of the mantle. *Tectonophysics*, **31**, 1–32.

Turnbull, D. (1956) Phase changes. *Solid State Phys.*, **3**, 225–306.

Vaughan, P.J. and Coe, R.S. (1981) Creep mechanism in Mg_2GeO_4: effects of a phase transition. *J. Geophys. Res.*, **86**, 389–404.

Vaughan, P.J., Green, H.W. II and Coe, R.S. (1984) Anisotropic growth in the olivine-spinel transformation of Mg_2GeO_4 under nonhydrostatic stress. *Tectonophysics*, **108**, 299–322.

Wu, T.-C., Bassett, W.A., Burnley, P.C. and Weathers, M.S. (1993) Shear-promoted phase transitions in Fe_2SiO_4 and Mg_2SiO_4 and the mechanism of deep earthquakes. *J. Geophys. Res.*, **98**, 19767–76.

[*Manuscript received 5 May 1997*]